

Off-axis performances of semi-analytical model analysis with the H.E.S.S. experiment

L. Rolland* and M. de Naurois*
for the H.E.S.S. collaboration

**Laboratoire de Physique Nucléaire et de Hautes Energies, IN2P3/CNRS, Universités Paris VI & VII, 4 place Jussieu, F-75252 Paris Cedex 05, France*

Abstract. The analysis method initially developed for the single telescope C.A.T. (Cerenkov At Themis) has been recently improved for stereoscopic observations with H.E.S.S. (High Energy Stereoscopic System). This method is based on an analytical model giving the light distribution resulting from a gamma-ray initiated shower in the atmosphere in the focal plane of the cameras. It simultaneously reconstructs the energy and source location of the initiating gamma-ray. Results of this method applied to H.E.S.S. Crab Nebula data are shown together with its spectrum. The potential of the H.E.S.S. experiment to analyse off-axis or extended source with this method is highlighted.

INTRODUCTION

The H.E.S.S. detector [1] is an array of four Imaging Atmospheric Cerenkov Telescopes, located in Namibia at 1800 meters altitude, designed to study very high energy (> 100 GeV) γ -rays. Each telescope is composed of a 107 m^2 mirror [2, 3] and a 5° diameter field of view camera [4].

The standard analysis is based on a fit of the image by an elliptical shape (the so-called Hillas parameters). An other method, based on an analytical model giving the light distribution resulting from a γ -ray initiated shower in the focal plane of the cameras, has been recently developed. After a short description of the method, it is applied to the 2003 Crab nebula data. The large field of view and the good angular resolution of the H.E.S.S. detector is an advantage to study extended sources. The performances of this analysis for off-axis observations are derived from simulations and off-axis Crab data from Spring 2004.

SEMI-ANALYTICAL MODEL

The principle of the semi-analytical model-based analysis is to compare actual shower images to analytical images, and derive from this comparison the primary shower parameters: energy E_γ , impact parameter D and γ -ray direction (zenith and azimuth angle). It had first been developed for the C.A.T. experiment [5].

Model

This model is based on the results from Hillas [6] where the mean development of electromagnetic showers is described and parametrized. Parametrizations of the number of charged particles (e^\pm) at a given atmospheric depth, their energy spectrum, angular distribution with respect to the shower axis and lateral distribution and spread around the shower axis are included in the model. The parametrizations are fitted with our Monte-Carlo simulations. The atmospheric characteristics such as density profile, optical absorption and Cerenkov emission properties are also taken into account. The detector features such as the mirror anisochronism, reflectivity and average PSF (Point Spread Function), the photomultiplier tubes quantum efficiency, and the integration window width are also included. In practice, the shower is divided into slices perpendicular to its axis at different depths. The contribution of every slices to the image is calculated. The output of the model is the mean number of photo-electrons in every pixels of the cameras for a shower of given energy, impact parameter observed at a given zenith angle.

The comparison between the mean images generated with the model and the data images is performed using a likelihood method. The likelihood is defined by the product over all the pixels i of the probability density function:

$$P_{DF}(x_i, \mu_i, \sigma_i) = \sum_n \frac{\mu_i^n e^{-\mu_i}}{n! \sqrt{2\pi(\sigma_{pi}^2 + n\sigma_\gamma^2)}} \exp\left(\frac{-(x_i - n)^2}{2(\sigma_{pi}^2 + n\sigma_\gamma^2)}\right)$$

The P_{DF} describes the probability of measuring x_i photo-electrons in pixel i when the theoretical signal is μ_i . The individual pedestal widths σ_{pi} take into account the fluctuations due to electronic noise and Night Sky Background (NSB). The photomultiplier tube resolution is described by σ_γ , n is the number of photo-electrons.

The sum is performed on every pixel of the cameras, and the NSB in every individual pixel is taken into account in the fit. Therefore, the model-based analysis does not need any prior image cleaning, lowering the energy threshold with respect to standard analysis. The relevant parameter is the goodness of fit:

$$g = \frac{\ln(\mathcal{L}) - \langle \ln(\mathcal{L}) \rangle}{N_{dof}} \quad (1)$$

with:

$$\langle \ln(\mathcal{L}) \rangle = \int_x \ln(P_{df}(x, \mu, \sigma_p)) \times P_{df}(x, \mu, \sigma_p) \times dx \quad (2)$$

From an analytical calculation, one can show that the distribution of this parameter should be centered on 0 with a width of $\sqrt{2/N_{dof}}$, where N_{dof} is the number of pixels used in the fit. Figure 1 gives its distribution for stereoscopic observations.

In contrast to other analysis, only one cut is used to select the gamma-like events: the maximum goodness of fit is set to 0.02. It gives a hadron rejection factor of the order of 50 with good flat γ -ray efficiency of the order of 80%. An additionnal cut on the γ -ray direction is used for point-like source analysis: the maximum square of the angular distance of the reconstructed γ -rays to the expected source position (θ^2) is set to 0.03°^2} . No dependence of these cuts on photon index and zenith angle are used.

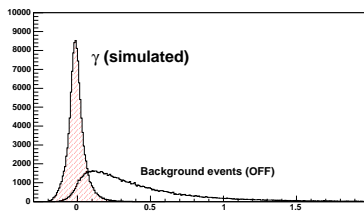


FIGURE 1. Distribution of the goodness of fit for stereoscopic observations: simulated γ -rays and background events from data.

For on-axis observations, energy resolution is of the order of 15%, angular resolution of the order of 0.06° [7]. The energy threshold in cuts at Zenith is 120 GeV (defined as the maximum differential flux for a E^{-2} spectrum). Off-axis performances are studied further.

Crab nebula analysis

The model-based analysis has been applied to a Crab nebula dataset of Fall 2003. This dataset consists in 4.0 live hours of 3-telescope observation at mean zenith angle of 46° . The trigger condition is 2.5 pixels above 4 photo-electrons per camera, with telescope multiplicity 2. The observations are in wobble mode, with declination offset of $\pm 0.5^\circ$. At this zenith angle, the model-based analysis gives an energy threshold of 480 GeV. Using a ring around the assumed source location to estimate the background, the excess is of 63σ (using Li&Ma [8] statistics) as shown in figure 2-Left. The apparent size of $0.063 \pm 0.001^\circ$ is compatible with expectations for a point-like source. The measured energy spectrum is shown figure 2-Right. Data are fit by a power law, $dN/dE = F_0 E_{TeV}^{-\alpha}$, with photon index $\alpha = 2.58 \pm 0.03$ and $F_0 = (34.2 \pm 0.7) \times 10^{-12} \text{cm}^{-2} \text{s}^{-1} \text{TeV}^{-1}$. Systematics errors are estimated to $\Delta\alpha \sim 0.15$ and $\Delta F/F \sim 15\%$. The reconstructed flux above 1 TeV is then $(2.17 \pm 0.06) \times 10^{-11} \text{cm}^{-2} \text{s}^{-1}$ which is in very good agreement with previous measurements [9] and standard H.E.S.S. analysis results [10].

OFF-AXIS PERFORMANCES

The off-axis performances of the model-based analysis have been derived from simulations. Results are then compared with the analysis of off-axis Crab data.

Simulation

Simulations of gamma-ray showers have been performed for fixed primary energies from 80 GeV to 20 TeV. Off-axis source directions have been simulated from 0.5° to 4.0° by step of 0.5° , for telescopes pointing toward the Zenith. Simulations of the

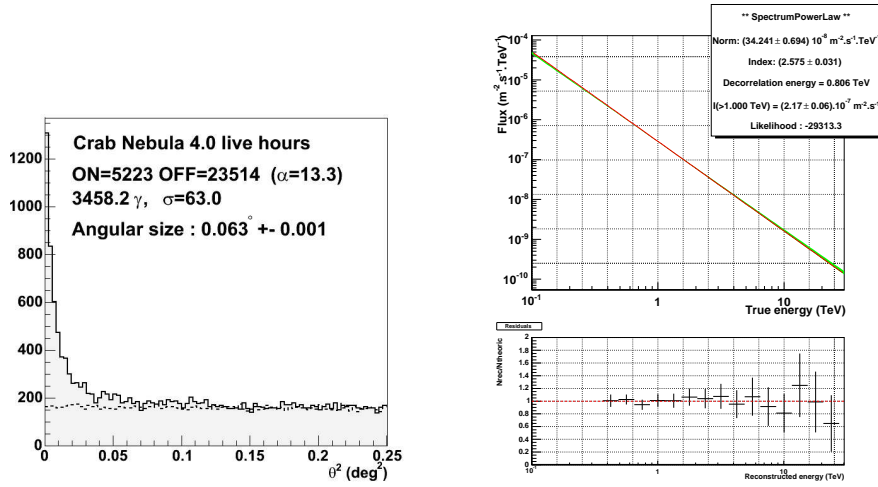


FIGURE 2. Left: Angular distribution of γ -ray like events relative to the location of the Crab nebula. θ is the angular distance between the γ -ray direction and the Crab nebula. A uniform background results in a flat θ^2 distribution. Dashed line: background region. Continuous line: signal region. Right: Crab nebula energy spectrum: dN/dE , computed with the method described in [11, 12]

H.E.S.S. detector have been performed with a trigger condition of 2.5 pixels above 4 photo-electrons per camera and a telescope multiplicity of 4.

The evolution of goodness of fit as function of energy is rather independent of the off-axis angle. A single cut value can then be used for the analysis. For multiplicity-4 analysis presented in this paper, we used a value of 0.02. Figures 3-Left, and 4 show the effective area, the energy resolution and the angular resolution at different energies and off-axis angles. They highlight that the model-based analysis performance are very stable for off-axis angles up to 2° . However, some effects are seen near the energy threshold and at high energy when the off-axis angle increases.

The energy threshold is of the order of 100 GeV for off-axis angles up to 2° , then increases to 300 GeV at 2.5° and to a few TeV at 4° : only high energy shower are indeed long enough to produce light inside the camera when they are 2.5° outside. Even 1.5° away, the effective area is still 25% of its value at the center.

The energy resolution and bias are defined as the sigma and the mean of a Gaussian fit of the distribution of the parameter $\ln(\tilde{E}/E)$, where \tilde{E} and E are the reconstructed and true energies. A θ^2 cut value of 0.02°^2 has been added. For off-axis angles up to the camera edges (2.5°), the resolution is stable of the order of 20%, and the bias is less than 10%. When off-axis angle is increased, the resolution is widened near the energy threshold and at high energy. The bias tends to increase also.

The distribution of the γ -ray reconstructed directions about the simulated direction is projected along one axis. It is fitted by a Gaussian whose mean and width give the angular bias and resolution. The resolution is stable up to 2.5° off-axis. It is between 0.05 and 0.08° for energies in the range $0.1 - 8$ TeV. It is up to 0.15° at higher energy. Angular resolution is still less than 0.15° for off-axis angles of 3.5° . The bias is flat, close to 0° , for off-axis angles up to 4° .

The performances of the model-based analysis derived from simulations are rather

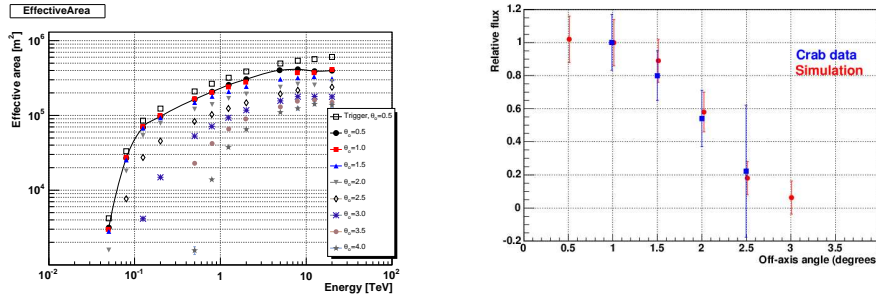


FIGURE 3. Left: The effective area at analysis level is shown for different off-axis angles between 0.5 and 4.0°. The empty squares give the trigger effective area at 0.5°. Right: The estimated integrated flux for a Crab-like source is compared to the H.E.S.S. data. Circles: simulation, Squares: Crab data.

stable up to 2.5°. A large fraction of the H.E.S.S. field of view might then be used in the analysis. This feature is of main importance to study diffuse γ -ray emission or extended sources.

Off-axis Crab nebula data analysis

The Crab nebula has been observed with wobble off-axis angles between 0 and 2.5° by step of 0.5° with H.E.S.S. between January and March 2004 with 4 telescopes. The telescope trigger condition was 2.5 pixels above 4 photo-electrons, and the telescope multiplicity 2. Only the 4-telescopes events have been used in the analysis.

Figure 5 shows the sky maps of the background events, gamma-like events and significance of the 2.5° off-axis data (1.7 live hours, 43° mean zenith angle). The sky acceptance with the 2 different pointings (offset in declination of -2.5 and 2.5 °) is clearly seen in the background event map. An excess of gamma-like events is visible on the border of the field of view of the H.E.S.S. telescopes.

The flux measured at different off-axis values is compared with simulations, assuming a power law spectrum of photon index 2.6 and flux at 1 TeV of $30 \times 10^{-12} \text{cm}^{-2} \text{s}^{-1} \text{TeV}^{-1}$. The relative fluxes, normalized to the flux at 1° off-axis, are drawn figure 3-right as function of the off-axis angle. Note that the Crab data have a mean zenith angle of about 46° whereas the effective area have been computed at Zenith. However, the relative flux evolution shows an agreement between data and simulations. For H.E.S.S., the Crab nebula is a point-like source. The angular resolution obtained on this source can thus be compared to simulations: the value of 0.7° is consistent with the results shown previously.

CONCLUSION

The model-based analysis has been developed and is now fully operational for the H.E.S.S. data analysis. It is based on the comparison between real event images and theoretical mean shower images in the cameras. Its main advantages compared to the

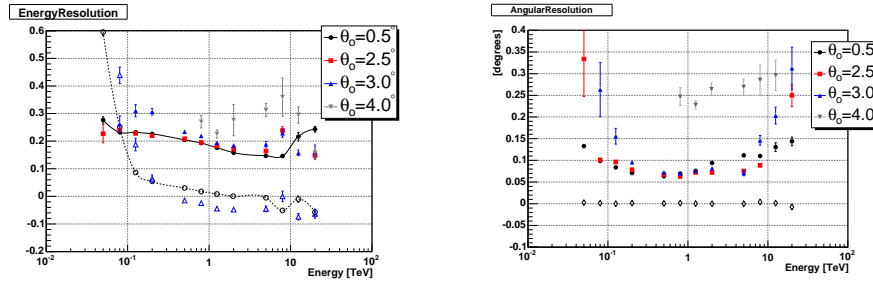


FIGURE 4. Left: The energy resolution evolution as function of energy is given at 4 different off-axis angles between 0.5 and 4.0°. The bias for angles 0.5 and 2.5° are also shown, between 10 and −10% above the energy threshold. Right: The angular resolution as function of energy is shown at different off-axis angles up to 4°. The empty diamonds gives the bias at off-axis angle 0.5°: it is close to 0° at every off-axis angles.

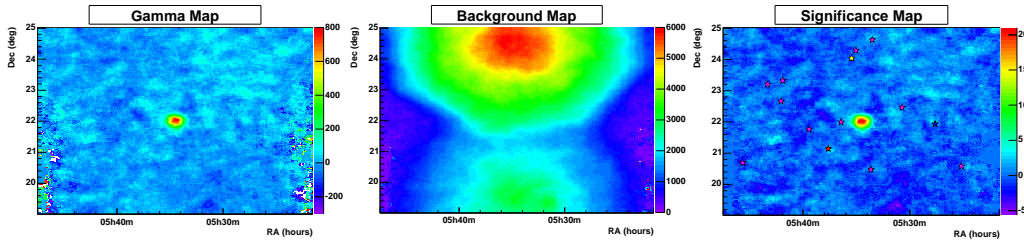


FIGURE 5. Sky maps of gamma-like events, background events and significance for 1.7 hours of Crab nebula data with wobble offset of $\pm 2.5^\circ$ in declination.

standard Hillas analysis are a lower threshold, a flatter γ -ray efficiency, and a better angular resolution. Results (flux and spectrum) obtained on the Crab data and other sources seen by H.E.S.S. are compatible with standard analysis.

The performances of the model-based analysis are very stable for off-axis angle observations up to 2 – 2.5°, which represents the entire H.E.S.S. field of view. This characteristics is of main importance to study extended sources or diffuse γ -ray emission.

REFERENCES

1. Hofmann, W., *Proc. 28th ICRC*, Univ. Academy Press, Tsukuba, Tokyo, 2003, pp. 2811–2814.
2. Bernlöhr, K. *et al.*, *Astropart. Phys.*, **20**, 111–128 (2003).
3. Cornils, R. *et al.*, *Astropart. Phys.*, **20**, 129–143 (2003).
4. Vincent, P. *et al.*, *Proc. 28th ICRC*, Univ. Academy Press, Tsukuba, Tokyo, 2003, pp. 2887–2890.
5. Le Bohec, S. *et al.*, *NIM*, **A 416**, 425 (1998).
6. Hillas, M., *Nucl. Phys.*, **8**, 1461–1473 (1982).
7. Lemoine-Goumard, M., *these Proceedings* (2004).
8. Li, T., and Ma, Y., *ApJ*, **272**, 317 (1983).
9. Aharonian, F. A. *et al.*, *ApJ*, **539-1**, 317–324 (2000).
10. Aharonian, F. *et al.* (H.E.S.S. collaboration), *Observation of the Crab Nebula with H.E.S.S.*, in prep. (2004).
11. Djannati-Atai, A. *et al.*, *Astron. Astrophys.*, **350**, 17–24 (1999).
12. Piron, F. *et al.*, *Astron. Astrophys.*, **374**, 895–906 (2001).